Modifying transcript lengths of cycling mouse segmentation genes

Michael Stauber, Christine Laclef, Annalisa Vezzaro, Mahalia E Page, David Ish-Horowicz

MECHANISMS OF DEVELOPMENT 129 (2012) 61–72

Available at www.sciencedirect.com

SciVerse ScienceDirect

journal homepage: www.elsevier.com/locate/modo

Modifying transcript lengths of cycling mouse segmentation genes

Michael Stauber [1], *Christine Laclef* [2], *Annalisa Vezzaro*, *Mahalia E. Page* [3], *David Ish-Horowicz* [*]

Developmental Genetics Laboratory, Cancer Research UK, London Research Institute, 44 Lincoln's Inn Fields, London WC2A 3LY, United Kingdom

ARTICLE INFO

Article history:
Received 5 December 2011
Received in revised form
16 January 2012
Accepted 17 January 2012
Available online 2 February 2012

Keywords:
Mouse genetics
Segmentation
Transcriptional elongation
Timing
Oscillators
Pattern formation

ABSTRACT

Regular production of somites, precursors of the axial skeleton and attached muscles is controlled by a molecular oscillator, the *segmentation clock*, which drives cyclic transcription of target genes in the unsegmented presomitic mesoderm (PSM). The clock is based on a negative feedback loop which generates pulses of transcription that oscillate with the same periodicity as somite formation. Mutants in several oscillating genes including the Notch pathway gene *Lunatic fringe* (*Lfng*) and the Notch target *Hes7*, result in defective somitogenesis and disorganised axial skeletons. Both genes encode negative regulators of Notch signalling output, but it is not yet clear if they are just secondary clock targets or if they encode components of a primary, pacemaker oscillator.

In this paper, we try to identify components in the primary oscillator by manipulating delays in the feedback circuitry. We characterise recombinant mice in which *Lfng* and *Hes7* introns are lengthened in order to delay mRNA production. Lengthening the third *Hes7* intron by 10 or 20 kb disrupts accurate RNA splicing and inactivates the gene. *Lfng* expression and activity is normal in mice whose *Lfng* is lengthened by 10 kb, but no effects on segmentation are evident. We discuss these results in terms of the relative contributions of transcriptional and post-transcriptional delays towards defining the pace of segmentation, and of alternative strategies for manipulating the period of the clock.

1. Introduction

Embryonic segmentation in vertebrates occurs as repeated production of mesodermal somites, the precursors of repetitive axial structures such as vertebrae, ribs and skeletal muscles. As the embryo grows posteriorly, bilateral pairs of somites arise at regular intervals from the cranial (anterior) region of the unsegmented presomitic mesoderm (PSM) at the tail end of the embryo (reviewed in Gossler and Tam (2002) and Tam and Trainor (1994)).

The periodicity of somite production varies between species (90 and 120 min in the chick and mouse, respectively). Nevertheless, in all vertebrates, somite formation is regulated by a molecular oscillator, the "segmentation clock", that

[*] Corresponding author. Tel.: +44 20 7269 3053; fax: +44 20 7269 3417.
E-mail address: david.horowicz@cancer.org.uk (D. Ish-Horowicz).
[1] Current address: Institut für Molekularbiologie, OE5250, Medizinische Hochschule Hannover, Carl-Neuberg-Str. 1, 30625 Hannover, Germany.
[2] Current address: UPMC Univ Paris 6, UMR 7622 CNRS, U969 INSERM, 9 Quai Saint Bernard, 75005 Paris, France.
[3] Current address: Wellcome Trust Centre for Stem Cell Research, University of Cambridge, Tennis Court Road, Cambridge CB2 1QR, United Kingdom.
0925-4773/$ - see front matter
doi:10.1016/j.mod.2012.01.006

drives cyclic gene transcription in the PSM with the same periodicity as somitogenesis (e.g. Aulehla et al., 2008; Masamizu et al., 2006) (reviewed in Dequéant and Pourquié (2008) and Lewis et al. (2009)). Inactivation or continuous expression of several of these cycling genes both cause irregular somitogenesis, suggesting that they have clock-related functions (e.g. Bessho et al., 2001b; Evrard et al., 1998; Serth et al., 2003; Zhang and Gridley, 1998).

The core mechanism of the oscillator that drives cyclic transcription is presumed to rely on a negative feedback loop whose period depends on delays within the individual steps of the circuit (Giudicelli et al., 2007; Lewis, 2003). Such steps could include those of mRNA synthesis (e.g. transcription, processing and nuclear export), and translation, post-translational modification and intracellular trafficking of the encoded proteins (Lewis, 2003). The period of the feedback loop and somite formation is a direct function of the sum of all such delays.

Many genes cycle in the mouse PSM, including several members of the Notch, Fgf and Wnt signalling pathways (Aulehla et al., 2003; Dequéant et al., 2006; Krol et al., 2011; Niwa et al., 2007, 2011), and several alternative negative feedback loops have been suggested to form the core of the clock (reviewed in Dequéant and Pourquié (2008), Giudicelli and Lewis (2004) and Pourquié (2011)). Nevertheless, the most likely group of models centre around components of the Notch signalling pathway. Notch activity cycling in the PSM is evolutionarily conserved between zebrafish and mammals (Henry et al., 2002; Holley et al., 2000; Jiang et al., 2000; Krol et al., 2011; Oates and Ho, 2002; Shankaran et al., 2007; Sieger et al., 2004), and dynamic Notch signalling is also seen during arthropod segmentation (Chipman and Akam, 2008; Pueyo et al., 2008; Schoppmeier and Damen, 2005; Stollewerk et al., 2003). Delayed autorepression of the *hairy*-related Notch target genes (*her1* and *her7* in zebrafish, *cHairy1* and *cHairy2* in chick, *Hes7* in mouse) is a potential Notch-related feedback loop (Bessho et al., 2003, 2001b; Hirata et al., 2004; Holley et al., 2002; Jouve et al., 2000; Lewis, 2003; Oates and Ho, 2002; Palmeirim et al., 1998). In the chick and mouse PSM, a Notch feedback loop could also involve the glycosyltransferase and Notch modifier Lunatic fringe (Lfng), which is activated by Notch signalling and in turn negatively regulates Notch activity (Aulehla and Johnson, 1999; Cole et al., 2002; Dale et al., 2003; Forsberg et al., 1998; McGrew et al., 1998; Morales et al., 2002; Morimoto et al., 2005).

In the mouse, an alternative feedback loop is formed by the Wnt signalling components Axin2 and Dkk1, which repress Wnt signalling and whose expression cycle (Aulehla et al., 2003; Dequéant et al., 2006; Krol et al., 2011), although levels of β-catenin protein do not cycle in the PSM (Aulehla et al., 2008; Dunty et al., 2008). Whether one or more of these negative feedback loops directs the clock is not yet certain. It remains possible that the clock comprises multiple linked oscillators (Dequéant et al., 2006; Krol et al., 2011; Niwa et al., 2007, 2011).

Many genetic alterations disrupt both cyclic transcription in the PSM and regular somite formation. However, such manipulations do not necessarily define the rate-defining, pacemaker oscillator; they could equally interfere with a secondary, slave oscillator. To identify components in the pacemaker circuit, one should show that modifying the kinetics of their synthesis and/or degradation alters (speeds up or slows down) the period of segment formation. Altered periodicity should affect somite length and, probably, the final number of somites and/or the axial length of the embryo. For example, slowing the clock down should generate fewer, larger somites, as has been reported for a zebrafish mutant with a slowed segmentation clock, and for mouse embryos with altered Notch signalling (Kim et al., 2011; Schröter and Oates, 2010). By contrast, modulation of downstream targets of the oscillator might affect somite morphology, but not their initial size or final number.

In this paper, we describe altering the transcriptional kinetics of the endogenous *Hes7* and *Lfng* genes to test if either reflects a rate-limiting component of a unique pacemaker circuit. We generate transgenic mice in which these genes are lengthened by insertion of 10 or 20 kb of exogenous DNA into an intron, in order to alter the transcriptional delay between initiating the genes' primary transcription and production of mature cytoplasmic mRNA. We show that the lengthened *Hes7* genes are inactive because the pre-mRNA transcripts are incorrectly processed, and lengthening *Lfng* has no obvious effects on somite formation or axial skeleton morphology. We relate these findings to recent results on the kinetics of transcriptional elongation and processing, and discuss the development of future tools for analysing the segmentation clock.

2. Results

2.1. *Generation of mouse lines with lengthened Hes7 or Lfng genes*

Cyclic accumulation of *Lfng* and *Hes7* transcripts is due to cyclic initiation of transcription (Bessho et al., 2003; Morales et al., 2002). To alter the time delay between transcriptional initiation and the generation of mature, translatable mRNA, we lengthened the genes by inserting exogenous sequence into an endogenous intron in order to retard completion of primary transcription without affecting mRNA and protein products. We based our construct design on an average consensus rate of transcriptional elongation by RNA polymerase II of ~1.2 kb/min, although measured rates vary widely (; 1.1–4.3 kb/min; Darzacq et al., 2007; Femino et al., 1998; e.g. Tennyson et al., 1995); reviewed in Swinburne and Silver (2008). On this basis, 10 kb insertion would increase the transcriptional delay by ~8 min. Mathematical modelling has indicated that the period of a negative-feedback oscillator is about twice the total delays in the negative-feedback circuit (Lewis, 2003); for a 10 kb insertion, this would correspond an increase of 16 min, or 14% of the normal 2 h cycle. The implications of recent, faster measurements of elongation rates (3.5–4.3 kb/min; Singh and Padgett, 2009) are examined in Section 3.

We lengthened the 3rd *Hes7* intron and the 1st *Lfng* intron in mouse embryonic stem cells by inserting 10 and 20 kb intron fragments from human *dystrophin* (*DMD*, Gene ID: 1756) that are distant from the *DMD* promoter and not expected to contain cis-regulatory elements active in the mouse PSM (Fig. 1A; Section 4.1). Injecting these targeted cells into mouse

blastocysts yielded mouse lines heterozygous for *Hes7* lengthened by 10 kb and 20 kb (referred to as *H10* and *H20*) and for *Lfng* lengthened by 10 kb (referred to as *L10*). We also recovered several stem cell lines with *Lfng* extended by 20 kb, but none incorporated into the germline.

For *H10* and *L10*, we tested expression of the lengthened genes by *in situ* hybridisation of heterozygous transgenic embryos with *dystrophin* intron-specific probes. Both lengthened genes cycle in the PSM like their wildtype counterparts (Fig. 1B–F). *L10* also shows a cranial stripe in the forming somite like that of the endogenous *Lfng* gene (Fig. 1B–D). Thus, the 10 kb insertion does not affect expression of either gene. We were unable to design effective *in situ* hybridisation probes for the 20 kb intronic insert, but analysis of heterozygous embryos with endogenous probes indicates that the transgene is also expressed in a similar manner to the wildtype gene (see below).

2.2. *Lengthened Hes7 mice are recessive lethal and deficient for Hes7 activity*

Heterozygous *H10* and *H20* are viable and fertile and resemble wildtype mice; only 3% of the adults show an overtly kinky tail (3/116, combined genotypes), a phenotype that can reflect locally perturbed segmentation. However, *H10* or *H20* homozygotes must die around birth because they are recovered as embryos from heterozygous parents in the expected proportion at E9.5–11.5 and E18.5 (18/106 *H10* and 36/156 *H20*), but not as adults (0/50; 0/108, respectively; Table 1). *H10* and *H20* are also unable to rescue the *Hes7* null phenotype in heteroallelic combination with the *Hes7* knock-out allele (Fig. 2I and not shown; Bessho et al., 2001b). Together, these results indicate that lengthening the intron has severely compromised Hes7 activity.

Analysis of transcription in homozygous *H10* and *H20* embryos by *in situ* hybridisation supports this conclusion. To monitor the lengthened genes specifically, we used an intronic *dystrophin* probe for *H10*, and the endogenous *Hes7* first intron probe for *H20*. In all cases, our results show that the transgenes are expressed constitutively throughout the PSM, as for inactive *Hes7* alleles (Figs. 1G and 2A; Bessho et al., 2003). This failure to cycle indicates that lengthening *Hes7* has disrupted the negative feedback required for oscillatory expression. The ectopic expression is recessive, i.e. not seen in the heterozygous embryos (Fig. 2B–D), indicating that it is due to reduced Hes7 activity.

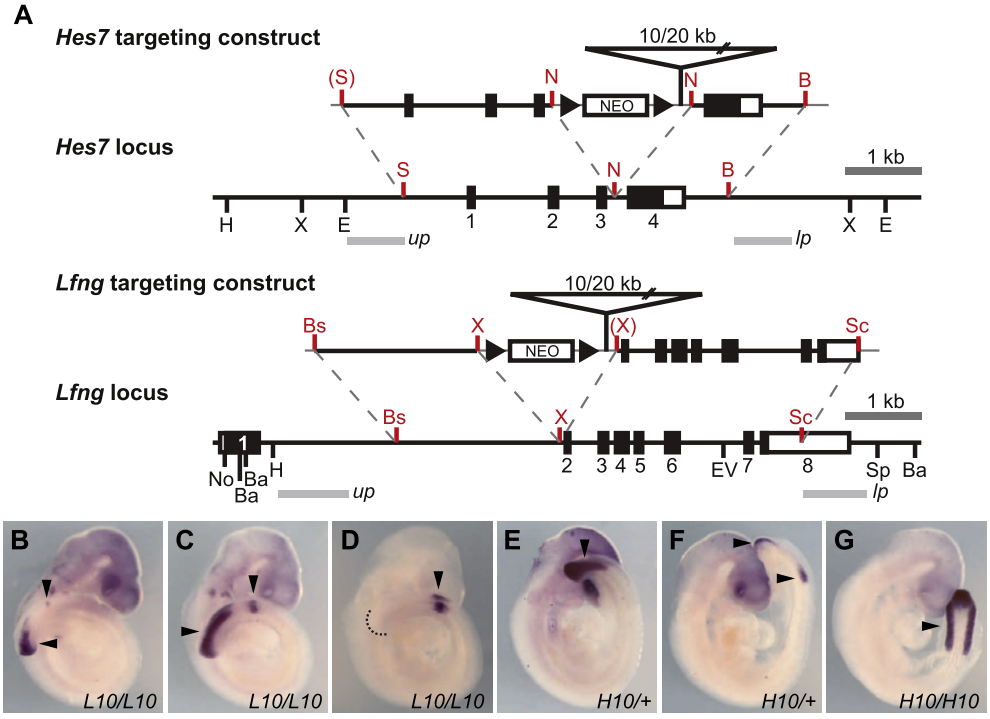

Fig. 1 – Generation of lengthened alleles of *Hes7* and *Lfng*. (A) Targeting strategy to insert 10 or 20 kb of intronic DNA into the 3rd intron of *Hes7* (top) or the 1st intron of *Lfng* (bottom). Exons are depicted as boxes and are numbered, ORFs shown in black. 10/20, 10 or 20 kb insert of human *dystrophin* intronic sequence; black triangles, *loxP* sites; NEO, *neomycin*^{r} gene; light grey boxes, position of probes (*up*, upstream probe; *lp*, downstream probe) used for Southern Blot analysis of embryonic stem cell clones; dashed lines indicate regions of potential recombination. Restriction sites used for production of targeting constructs are shown in red, restriction sites used for Southern Blot analysis in black: B, Bsu36I; Ba, BamHI; Bs, BssHII; E, EcoRI; EV, EcoRV; H, HindIII; N, NcoI; No, NotI; S, StuI; Sc, SacI; Sp, SpeI; X, XbaI. Restriction sites in brackets are disrupted after ligation. (B–G) Transcription of lengthened *L10* and *H10* in ~E9.5 embryos visualised with a riboprobe against the 10 kb human *dystrophin* intronic insert; arrowheads point at transgene expression domains in the PSM. Transcription is dynamic in the PSM of *L10/L10* (B–D; *n* = 28) and *H10/+* (E and F; *n* = 13), but ubiquitous in *H10/H10* (G; *n* = 4). A dotted line marks the caudal end of the embryo in D.

Table 1 – Breeding statistics of heterozygous *Hes7* knock-in mice: viability of homozygous *H10* and *H20* at various stages.

Stage	Line	Number of homozygous offspring	Number of heterozygous offspring	Number of wildtype offspring	Total offspring analysed	Numbers of litters analysed
E9.5–11.5	*H10*	12	53	22	87	6
	H20	31	73	33	137	9
E18.5	*H10*	6	8	5	19	2
	H20	5	9	5	19	2
P0	*H10*	0	34	16	50	8
	H20	0	68	40	108	10

H10 and *H20* also show null-like segmentation phenotypes. Heterozygous embryos exhibit regular, essentially wildtype vertebral columns, rib cages with a normal number of vertebrae, and ribs and only very occasional minor pattern irregularities (Fig. 2G). By contrast, homozygous E11.5 embryos show uneven segmentation throughout the body axis, as marked by expression of the caudal somite marker *Uncx4.1* (Fig. 2E and F; Mansouri et al., 1997). Homozygous *H10* and *H20* E18.5 embryos show extensive and severe malformations and multiple fusions of ribs and of vertebrae, and truncated tails (e.g. Fig. 2H).

These phenotypes are more severe than those of the $Hes7^{BAP}$ allele (Stauber et al., 2009), in which weak residual activity is sufficient for the development of regular sacral vertebrae. Sacral vertebrae are disrupted in homozygous *H10* and *H20* embryos (Fig. 2H and not shown), indicating that the lengthened alleles are essentially null.

2.3. *Lengthening the 3rd Hes7 intron disrupts splicing and inactivates Hes7*

To study why lengthened *Hes7* is inactive, we examined transcript structures in heterozygous and homozygous embryos, using reverse transcription and PCR (RT-PCR) with primers in exons 1 and 4 (last) that amplify a 620 bp product from wild-type transcripts (Fig. 2J). From heterozygous *H10* and *H20* embryos, we obtained the wildtype fragment and a 532 bp product which was revealed by DNA sequencing to derive from transcripts that precisely lack the 88 bp 3rd exon ($Hes7^{\Delta ex3}$: Fig. 2K, Table 2). Homozygous *H10* and *H20* embryos contain only the shortened, mis-spliced product ($n = 43$, $n = 46$, respectively; Fig. 2K; Table 2), showing that lengthening the intron has caused exon-skipping. This failure to splice appears to be a consequence of the insertion site within the third *Hes7* intron, because the same sequence inserted in *Lfng* intron 1 does not affect maturation of *Lfng* transcripts (see below).

Hes7 protein is a transcriptional repressor, with a basic-helix–loop–helix domain that mediates dimerisation and DNA-binding, and a C-terminal WRPWP motif that mediates repression. Lack of exon 3 (which mainly encodes the second helix; Bessho et al., 2001a) would cause a translational frameshift so as to encode a truncated protein in which the basic, DNA-binding domain and the first helix are fused to 60 out-of-frame aminoacids from exon 4. This fusion protein is almost certainly inactive, consistent with the null-like perinatal phenotypes of homozygous *H10* and *H20* embryos.

Primary transcripts from the mutant gene are mis-spliced in additional ways that also preclude encoding of an active protein. Some transcripts are processed but retain stretches of the lengthened intron 3 so that translation would be truncated. These RNAs are too long to be detected in the above PCR reactions, but are revealed by RT-PCR between exon 1 and a site within the *dystrophin* insertion sequence in *H10* (Fig. 2J, blue arrows).

In wildtype embryos, most *Hes7* transcripts are correctly spliced (Fig. 2K), although DNA sequencing of RT-PCR products shows that transcripts lacking exon 3 are also occasionally present (Fig. 2K, Table 2). Other rare defective products correspond to transcripts lacking the last 13 nt of the 3rd exon (generated by using an alternative 5′ splice site consensus GT within exon 3), or with an insertion of 5 nt between exon 3 and 4 (Table 2). Both forms would cause frameshifts and truncated translation in exon 4. These findings indicate that splicing between wildtype *Hes7*'s exons 3 and 4 is inherently error-prone, and raise the possibility that lengthening intron 3 aggravates a pre-existing unreliability.

Lengthening the intron may also affect other aspects of transgene transcription. *In situ* hybridisation with *dystrophin* and *Hes7* intron probes indicates that the primary transcription rates of *H10* and *H20* are relatively normal (e.g. Fig. 1E and F; Fig. 2B–D). Nevertheless, $Hes7^{\Delta ex3}$ is consistently amplified more efficiently from *H10/H10* than from *H20/H20* embryos (Fig. 2K). *H20* transcripts might be elongated more slowly than *H10* or, more likely, are mis-spliced predominantly into transcripts that are too long to be amplified by exon 1 and 4 PCR primers.

Altogether, our results indicate that *H10* and *H20* mice cannot be used to study the kinetics of the segmentation clock as intended. Rather, they illustrate the unpredictable effects of altering intron structure and length.

2.4. *Lengthening Lfng does not affect somite number or skeleton length*

Lengthening *Lfng* by 10 kb appears not to affect expression or activity, unlike the equivalent manipulation of *Hes7*. *L10* transcript levels are normal in homozygous embryos as judged by *in situ* hybridisation (Fig. 3A–D), and only wildtype RT-PCR products are amplified using primers between exons 1 and 4 ($n = 30$; Fig. 3E).

Similarly, homozygous *L10* embryos and adults are viable and morphologically wildtype. Somite compartmentalisation appears regular, and markers for the caudal and cranial somite-halves, *Uncx4.1* and *Tbx18* (Kraus et al., 2001) respectively, are expressed in regular stripes along the length axis

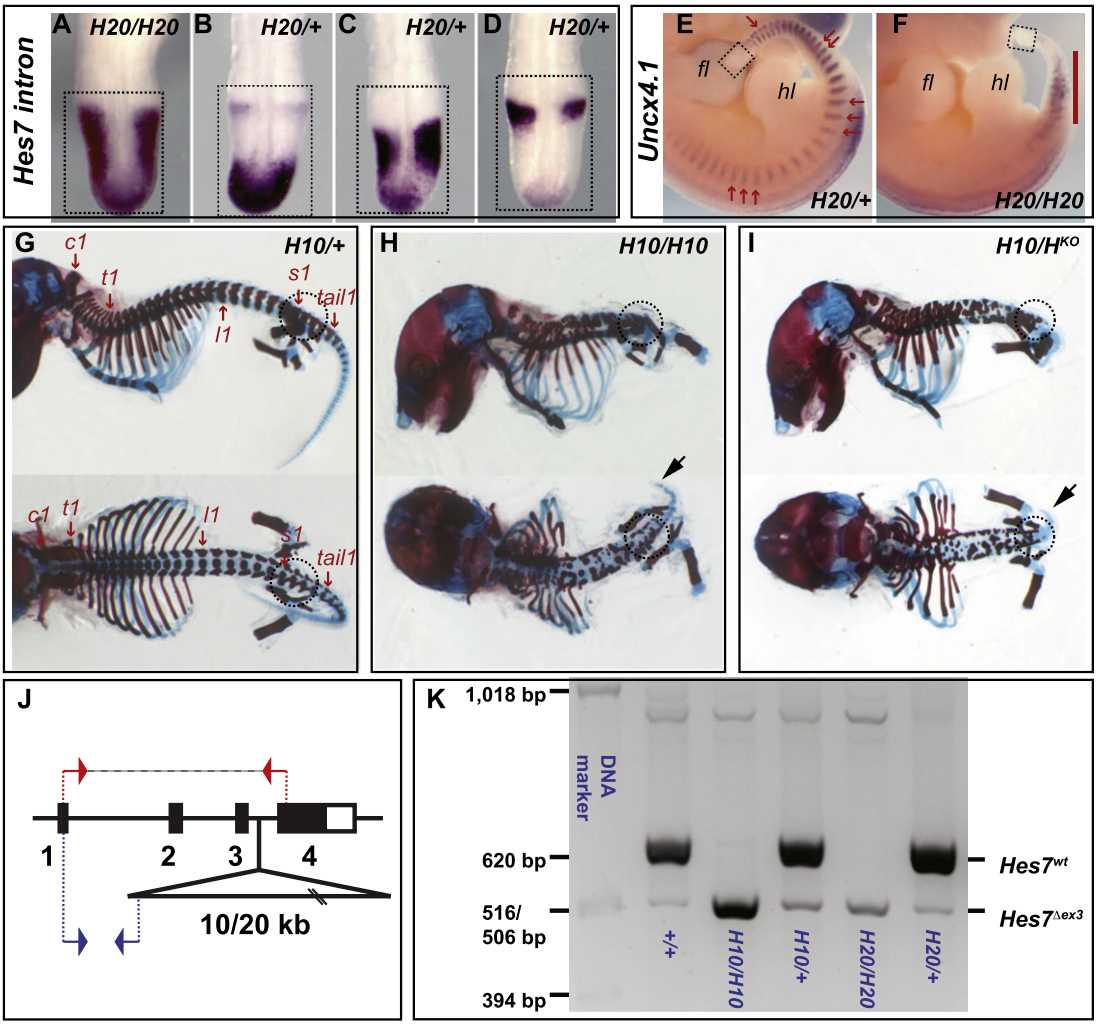

Fig. 2 – Error-prone splicing of *Hes7* is completely disrupted in the lengthened alleles. (A–D) Visualisation of *Hes7* transcription with an *Hes7* intron probe shows that the gene is oscillating in heterozygous (B–D, *n* = 9 *H20/+*; *n* = 9 *H10/+* not shown), but not in homozygous (A, *n* = 7 *H20/H20*; *n* = 7 *H10/H10* not shown) *H20* embryos. (E and F) Segmentation of the embryo, visualised with the segment marker *Uncx*4.1, is normal in heterozygous *H20* (*n* = 8 *H20/+*; *n* = 3 *H10/+* not shown), but severely disorganised in homozygous *H20* E11.5 embryos (F, *n* = 7 *H20/H20*; *n* = 3 *H10/H10* not shown). PSMs are boxed in A–F; red arrows point at examples of regular *Uncx*4.1 stripes; red bar in F marks irregular *Uncx*4.1 expression; *fl*, forelimb, *hl*, hindlimb. (G–I) E18.5 skeleton preparations show the normal skeleton formed by *H10/+* mice (G, *n* = 8 *H10/+*; *n* = 9 *H20/+* not shown) and the disorganised skeletons of *H10/H10* (H, *n* = 6 *H10/H10*; *n* = 5 *H20/H20* not shown) and *H10/Hes7*^{KO} (I, *n* = 8 *H10/Hes7*^{KO}; *n* = 3 *H20/Hes7*^{KO} not shown). Lateral (top) and dorsal (bottom) views of the same skeletons are shown; red arrows indicate exemplary regular vertebrae in G (*c*1, *t*1, *l*1, *s*1, *tail*1 are the first cervical, thoracic, lumbar, sacral and tail vertebrae); circles highlight the sacral area, which shows no regular vertebrae in (H and I); black arrows point at the truncated tails in (H and I). (J) Positions of *Hes7* RT-PCR primers: red primers amplify exon1–exon4 of the *Hes7* cDNA; blue primers amplify exon1–lengthened intron 3 of incompletely spliced RNA/cDNA. (K) Products of RT-PCR with red primers (see J) on total RNA from individual embryos of the genotype indicated separated on an agarose gel. In all experiments, *H10* and *H20* gave essentially the same results.

(Fig. 3F and G). The axial skeletons of *L10/+*, *L10/L10* and *L10/Lfng*$^{-}$ E18.5 foetuses (*n* = 9, 25 and 5, respectively), are regular, long-tailed, and indistinguishable from wildtype (Fig. 3H and not shown).

The lengths of newly-formed *L10/L10* somites are also unaffected. We labelled caudal compartments by *in situ* hybridisation with *Uncx*4.1 (e.g. Fig. 4A–F) and determined the average length of the three youngest somites in individual embryos. The averages were slightly longer in *L10/L10* than wildtype embryos (*n* = 11 and 7, respectively) but the difference is not statistically significant (Fig. 4G, Table 3).

We also tested if shortening *Lfng* transcripts leads to shorter somites, using embryos in which a chick *Lfng* cDNA (*cLfng*) is expressed from a mouse *Lfng* cycling promoter (5kL lines, Stauber et al., 2009). *cLfng* primary transcripts are 5.7 kb shorter than wildtype and include only a single intron (Section 4.2), and so might be expected to suffer a shorter transcriptional delay. Nevertheless, we found no significant difference in so-

Table 2 – Frequencies of different *Hes7* splice variants sequenced.

Genotype	Number of clones	Wildtype (620 bp)	$Hes7^{\Delta ex3}$ [a] (532 bp)	$Hes7^{\Delta 13nt}$ [b]	$Hes7^{+5nt}$ [c]
+/+ [d]	42	16	23	2	1
H10/H10	43	0	43	0	0
H10/+	25	6	19	0	0
H20/H20 [e]	46	0	46	0	0
H20/+	20	5	13	2	0

[a] Exon 3 missing. The apparent excess of $Hes7^{\Delta ex3}$ to $Hes7^{wt}$ clones recovered for wild-type and heterozygous embryos is probably because of differential purification or cloning efficiency (and contrasts with the gel in Fig. 2K).
[b] 13 Last nt missing at 3′ end of exon 3 (GTGGAGCCCCCGG).
[c] 5 nt inserted between exon 3 and exon 4 (GTACA, which exists in the 3rd intron, 324 bp downstream of the 3rd exon).
[d] Combined data from individual amplifications of total RNA independently prepared from 5 +/+ embryos. $Hes7^{\Delta ex3}$ was isolated from all 5 +/+ embryos.
[e] Combined data of RT-PCRs on total RNA independently prepared from 2 *H20/H20* embryos.

mite length between wildtype and *cLfng;Lfng*$^{-/-}$ embryos, which express only *cLfng* ($n = 4$; 5*kL*/0 in (Stauber et al., 2009); Fig. 4E–G, Table 3). Nor are there differences in the numbers of each vertebrae type, or the lengths of the vertebral column or individual body regions between *L10/+*, *L10/L10*, wildtype and *cLfng*^{cDNA} E18.5 foetuses (Fig. 4G, Table 4).

As a potentially more sensitive test of altered clock period, we examined the total number of somites in E13.5 embryos, when somitogenesis is just ceasing. If *L10* were to lengthen clock period, one might expect a corresponding reduction in the total somite number (e.g. by 9 somites (14%) if a 10 kb insert were to cause an 8 min delay). Altering clock period in the zebrafish affects segment number in such a manner, indicating that terminating segmentation is independent of the clock (Schröter and Oates, 2010).

To count somite number, we made use of high resolution episcopic microscopy (HREM,<http://www.embryoimaging.org>; Weninger et al., 2006; Weninger and Mohun, 2007) to visualise the entire length of the body axis of embryos at E13.5 when somitogenesis has ceased (Gossler and Tam, 2002; Sewell and Kusumi, 2007). In summary, embryos were embedded in fluorescent methacrylate resin, sectioned under the microscope, and a surface image captured after each section. The resulting digital image series was converted to a volume data set in order to count total somites (Section 4.6).

Accurate counting reveals that lengthening *Lfng* does not affect the total number of somites formed. Homozygous *L10* embryos and control, sibling heterozygotes develop similar numbers of somites (63.0 ± 1.0, $n = 3$ and 63.3 ± 1.7, $n = 4$, respectively) (Movies S1–S6, Fig. 4H–M), equivalent to the number in *C57Bl/6J* wild-type embryos (63.7 ± 0.6 somites, $n = 3$) and other, unrelated mouse embryo strains (A.Vezzaro. and T. Mohun, unpublished data). These results show clearly that lengthening *Lfng* primary transcripts by 10 kb does not cause a significant delay in segmentation clock period.

3. Discussion

3.1. *Lengthening Hes7 causes mis-splicing*

In this paper, we characterise transgenic mice in which the endogenous *Hes7* and *Lfng* genes were lengthened to delay their transcription. However, inserting 10 or 20 kb of exogenous *dystrophin* DNA into a *Hes7* intron caused mis-splicing and premature translational termination, thereby inactivating the lengthened gene. By contrast, expression of the *Lfng* gene lengthened by 10 kb was normal, as is segmentation of the homozygous animals. We discuss the relevance of these results in terms of the kinetics of transcription, effects on somite size and number, and future strategies for studying the segmentation oscillator.

We targeted mouse *Hes7* for lengthening because the gene is strongly implicated in regulating embryonic segmentation, both as an output of the clock and also as a candidate component of the clock circuitry (Bessho et al., 2003, 2001b; Hirata et al., 2004; Niwa et al., 2007, 2011; Takashima et al., 2011). Indeed, dynamic expression of *hairy*-related genes in precursor tissue is a consistent feature of segmentation in vertebrates and in several invertebrates (see Section 1). However, both of our intron-insertion constructs essentially inactivated the gene, as evidenced by the null-like somitic and skeletal phenotypes (Fig. 2F, H and I), and the complete lack of correctly-spliced *Hes7* mRNA in homozygous mutant embryos (Table 2). Both lengthened *Hes7* alleles are transcribed in wildtype patterns, as judged by *in situ* hybridisation on heterozygous embryos (Figs. 1E and F and 2B–D), but their transcripts are incorrectly spliced to encode truncated proteins that lack critical dimerisation and corepressor-binding domains (Bessho et al., 2001a).

Hes7 mis-splicing is not due to sequences within the 10 kb *dystrophin* insertion because it does not cause mis-processing when inserted into *Lfng*. Rather, the defective *Hes7* processing must be due to the site of insertion. The targeted *Hes7* intron is much shorter than that of *Lfng* (312 vs 4005 bases); perhaps the short intron is selectively unable to tolerate extreme (30-fold for *Hes7*) lengthening. Alternatively, the insert might interrupt specific *cis*-acting sequences required for splicing of *Hes7* exon 3.

3.2. *Lengthened Lfng segments normally*

By contrast, lengthening *Lfng* by 10 kb affects neither its expression nor somite formation. Somite length, vertebrae number, and axial skeleton length and proportion are normal in homozygous *L10* embryos (Figs. 3F–H, 4G), indicating that segmentation is normal. In particular, somite counts by HREM

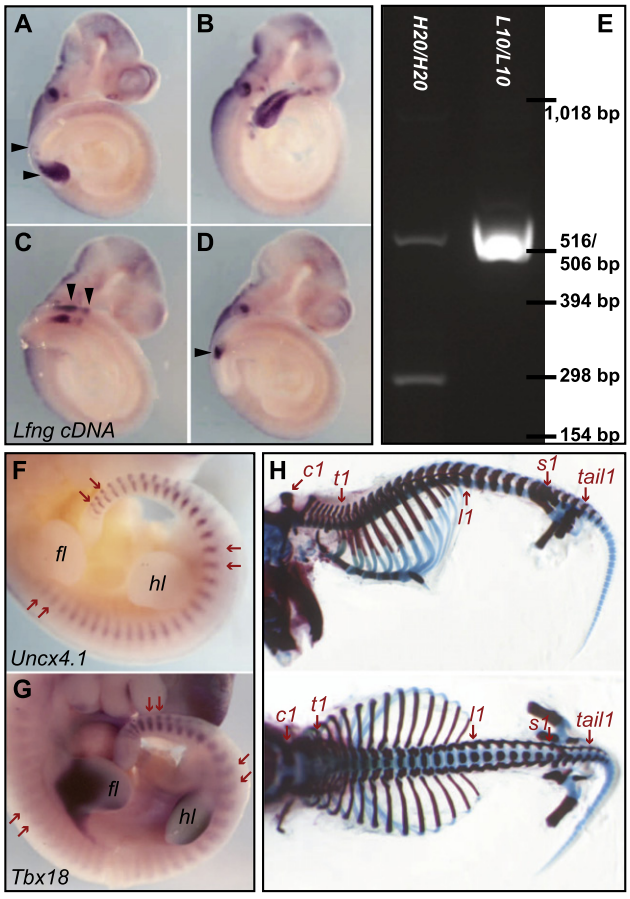

Fig. 3 – Normal somitogenesis in *L10/L10* embryos. (A–D) *Lfng* mRNA, visualised by *in situ* hybridisation with a *Lfng* cDNA probe, shows dynamic expression in the PSM of *L10/L10* E9.5 embryos (arrowheads point at *Lfng* expression domains in the PSM). (E) Agarose gel of RT-PCR products amplified from total RNA from individual embryos using primers from *Lfng* exons 1 and 4; the *Lfng* wildtype RT-PCR product is 562 bp; the side-product present in the *H20/H20* lane (which is wildtype for *Lfng*) is described in Section 4.5. (F and G) Regular domains of the caudal somite marker *Uncx4.1* (F) and the cranial somite marker *Tbx18* (G), visualised by *in situ* hybridisation to *L10/L10* E11.5 embryos, indicate that regular somites (e.g. red arrows) have been generated. *fl*, forelimb; *hl*, hindlimb. (H) Axial skeletons of *L10/L10* E18.5 foetuses are regular and indistinguishable from wildtype; a lateral (top) and dorsal (bottom) view is shown; see legend to Fig. 2G for annotations.

shows that *L10* embryos develop normal numbers of somites (Fig. 4H–M, Movies S1–S6). Comparative studies of mouse, chicken, corn-snake and, particularly, zebrafish indicate that this total is controlled separately from clock periodicity itself, and that small differences in clock period can lead to significant alterations in somite number, in particular in the tail (Gomez et al., 2008; Schröter and Oates, 2010). *L10/L10* have a normal number of somites at E13.5, the time by which somitogenesis has ceased, indicating that the period of the segmentation clock has not been affected.

One explanation for this result is that *Lfng* is not a clock component, and that its cyclic expression is driven by an upstream, *Lfng*-independent oscillator. Indeed, requirements for *Lfng* during segmentation seems to vary along the body-axis, being essentially dispensable in the sacral region (Shifley et al., 2008; Stauber et al., 2009). Several signalling pathways cycle during segmentation (Dequéant et al., 2006; Krol et al., 2011), any of which could represent a pacemaker clock that drives the others' oscillations.

Alternatively, *Lfng* oscillations might contribute to the clock but not be rate-limiting. The clock could involve redundant oscillators that can compensate for each other, either completely or partially, so that modulating the kinetics of *Lfng* expression has only subtle effects on the clock. Kim et al. (2011) recently showed that upregulation of mouse Notch activity (by loss of its repressor Nrarp) extends the period of the segmentation clock causing formation of fewer somites, while repression of Notch (with a γ-secretase inhibitor) has the opposite effect. These results are consistent with Notch signalling being an integral aspect of the segmentation clock.

As we did not detect changes in somite number in *L10/L10* embryos it is likely that transcriptional elongation is not rate-limiting for Lfng expression. This explanation is supported by a recent reappraisal of vertebrate transcriptional kinetics measured during recovery from inhibiting progression from transcriptional initiation to elongation (Singh and Padgett, 2009). Our transgenic experiments were based on a previous consensus elongation rate of 1.2 kb/min (Femino et al., 1998; Lewis, 2003; O'Brien and Lis, 1993; reviewed in: Swinburne and Silver (2008) and Tennyson et al. (1995)), whereby a 10 kb increase in primary transcript length would delay transcription by 8 min and lengthen clock period by about 16 min (Lewis, 2003). However, analysis of a wide variety of endogenous human genes showed them to be elongated 3-fold faster at 3.8 kb/min (Singh and Padgett, 2009). At such speeds, a 10 kb insertion would delay transcriptional elongation by less than 3 min and the period of the clock by only 5 min, i.e. by less than 5% (Lewis, 2003). Shortening transcripts by less than 6 kb (as in *cLfng;Lfng*$^{-/-}$ embryos) would also not be expected to affect the timing of segmentation significantly.

3.3. *Strategies for altering clock period*

Despite our inability so far to alter clock periodicity, altering candidate delay processes remains the best strategy for defining clock components and circuitry. In principle, one could attempt to lengthen or shorten other steps of macromolecular synthesis (e.g. protein translation, modification or stability). However, the kinetics of these processes are even more poorly understood than that of transcription, and thus even more difficult to manipulate predictably. For example, Hirata et al. introduced into transgenic mice a *Hes7* point mutation that increases the protein's half-life in cultured cells without affecting its activity (Hirata et al., 2004). However, the mutant mice show a recessive *Hes7* null-like phenotype in which cyclic expression is lost, leaving open whether this phenotype is due to altering pacemaker kinetics or to loss of *in vivo* repressive activity.

Another implication of the recent reassessment of transcriptional elongation kinetics is that RNA processing may

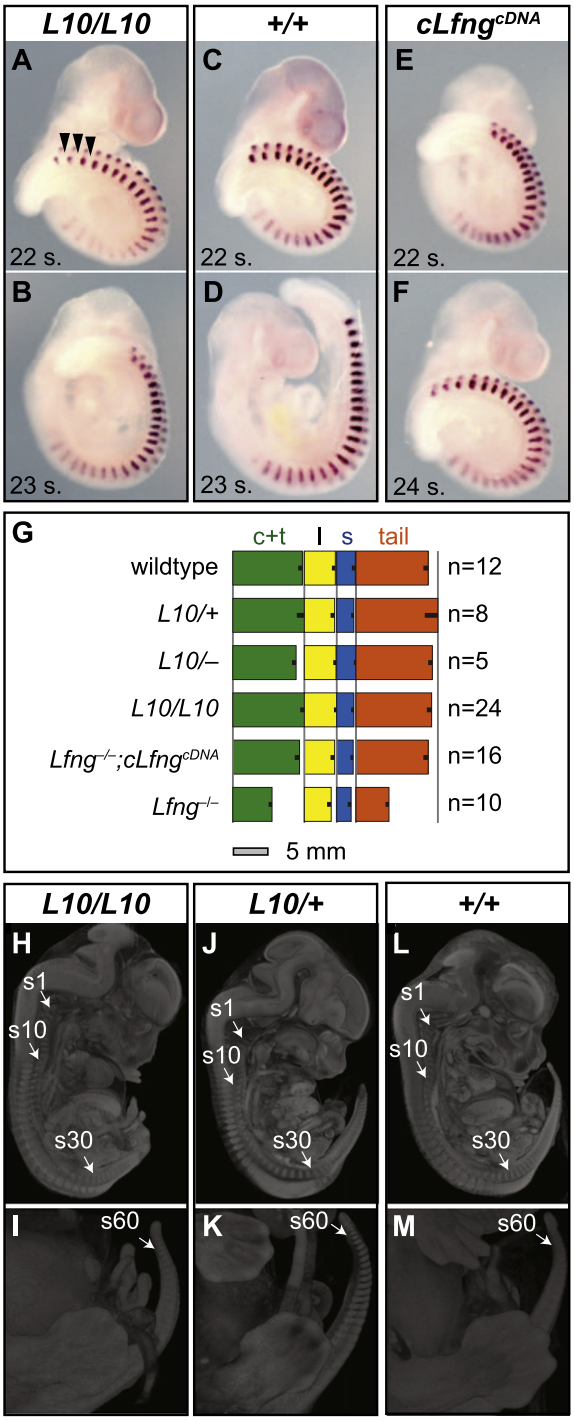

Fig. 4 – Wildtype-like segmentation after lengthening and shortening of *Lfng*. (A–F) Examples of embryos labelled with *Uncx4.1* caudal somite marker for simple measurement of somite length. Genotype and developmental stage [22, 23, or 24 somite (s.) stages] are indicated. All embryos were processed, stained, and photographed in parallel without changing the settings, so that their images can be used for direct size comparisons. (G) Length of the axial skeleton of wildtype, *L10/+*, *L10/Lfng*$^{-}$, *L10/L10*, homozygous *cLfng*^{cDNA};*Lfng*$^{-/-}$ and *Lfng*$^{-/-}$ E18.5 foetuses (for an exemplary image see Fig. 3H). Cervical and thoracic (c + t; green), lumbar (l; yellow), sacral (s; blue) body region and tail (orange) are depicted separately and aligned to the left for easier comparison of length. Numbers of skeletons analysed is given on the right. Error bars (standard deviation) are shown on the right side of each box (only the left arm of the error bar extending inside the box is shown); c.f. Table 4; data for wildtype, *cLfng*^{cDNA};*Lfng*$^{-/-}$ and *Lfng*$^{-/-}$ are taken from Stauber et al. (2009). (H–M) Examples of E13.5 embryos imaged via HREM for somite count (see also Movies S1–S6). Genotype is indicated. (H, J and L) Side view of the trunk region, the 1st, 10th and 30th somites are indicated (arrows). (I, K and M) Side view of the tail region, the 60th somite is indicated (arrows).

Table 3 – Relative somite lengths in wildtype, *L10/L10* and *clfng*^{cDNA};*lfng*$^{-/-}$ embryos at 20–27 somite stages.

Embryonic stage (somite number)	20	21	22	23	24	25	26	27
Wildtype	n.d.	2.0 ± 0.2; 2.1 ± 0.4	2.6 ± 0.2	2.3 ± 0.1	n.d.	2.8 ± 0.1; 2.6 ± 0	3.1 ± 0.2	n.d.
L10/L10	1.9 ± 0	2.4 ± 0.2	2.7 ± 0.2	2,2 ± 0.1	2.6 ± 0.2	3.2 ± 0.1; 2.8 ± 0.1; 3.1 ± 0.3; 3.0 ± 0.1	3.3 ± 0.4; 3.1 ± 0.1	n.d.
cLfng^{cDNA};*Lfng*$^{-/-}$	n.d.	n.d.	2.0 ± 0.1	n.d.	2.7 ± 0.1	2.6 ± 0.1	n.d.	3.2 ± 0.6

Each measurement corresponds to the average length (in mm; mean ± SD) of the last three somites sI, sII, sIII of an individual embryos at the embryonic stage indicated, taken from a magnified image of *Uncx4.1* stained embryos. n.d., not determined. $n = 22$.

Table 4 – Comparison of the length of body regions and the number of tail vertebrae in *L10/+*, *L10/L10* and *L10/Lfng*$^{-}$ E18.5 skeletons.

	L10/+	*L10/L10*	*L10/Lfng*$^{-}$
Number of E18.5 skeletons analysed	8	24	5
Length of whole vertebral column (mm)	29.4 ± 1.3	28.7 ± 0.9	27.8 ± 0.5
Length of cervical + thoracic region (mm)	10.4 ± 1.1	10.4 ± 0.6	9.2 ± 0.6
Length of lumbar region (mm)	4.4 ± 0.6	4.7 ± 0.4	4.6 ± 0.4
Length of sacral region (mm)	2.8 ± 0.4	2.5 ± 0.4	2.8 ± 0.3
Length of tail (mm)	11.9 ± 1.0	11.0 ± 0.7	11.1 ± 0.6
Number of tail vertebrae [a]	29.9 ± 1.2	29.0 ± 1.0	30.0 ± 0

[a] Number of cervical (7), thoracic (13), lumbar (6) and sacral (4) vertebrae was normal in mice of all genotypes except for one missing lumbar vertebra in an *L10/+* and two *L10/L10* foetuses, a phenotype also occasionally observed in wildtype mice.

Table 5 – List of primers used for genotyping mice.

Genotype	Sequence of primer pair
neo	TGGGCACAACAGACAATCGGCTGCTCTG
	CGGCAAGCAGGCATCGCCATGGGTC
cre	AGAAAACGTTGATGCCGGTGAACG
	CAGCCACCAGCTTGCATGATCTCC
10 kb *dystrophin* insert	GGGTAAACAGGAACGCTTCAGG
	CCATGGGAAAAGCAAACTGACC
20 kb *dystrophin* insert	CCAATTGGCTGAAAGCAAAAGG
	ATGGTGCAAGGATTGGAATTGG
Wildtype *Hes7* (flanking intron insertion site)	CGAAGCTGGAGAAAGCGGAGAT
	CGGAAGCCGGACAAGTAGCAG
Wildtype *Lfng* (flanking intron insertion site)	CTGGCAGGCTGTGTCAATAAGG
	CGAGTGAACTGGCCTCTTAGCC
Hes7^{lacZ} KO allele[a]	AGAAAGGGCAGGGAGAAGTGGGCGAGCCAC
	TTGGCTGCACCCCGGGGGATCCACTAGTTC
Wildtype *Hes7* (i.e. lacking *lacZ* insertion)[a]	AGAAAGGGCAGGGAGAAGTGGGCGAGCCAC
	GTTCTGAGAGCGAGAGGGGGTCTGGGATGG
neo^{r} insertion in *Lfng* KO allele	ACCGCTTCCTCGTGCTTTACG
	AGGAACAAATATGGCCATTCACTCC

a *Hes7* primer sequences kindly provided by Hiromi Hirata, Kyoto University.

prove to be a rate-limiting step in generating mature transcripts. Singh and Padgett show that intron splicing takes 5–10 min, for a wide range of sizes (between 1.2 and 243 kb; Singh and Padgett, 2009). If elongation and processing of clock genes in the PSM were to show similar *in vivo* kinetics, delays associated with RNA splicing, especially of the 3′-most intron(s), might contribute more to determining clock period than transcriptional elongations. Indeed, evidence for this

view comes from a recent paper in which cyclic expression of an intronless *Hes7* gene in transgenic mice disrupts both the clock and segmentation (Takashima et al., 2011). For these reasons, it will be important to measure accurately the *in vivo* kinetics of elongation, processing and export of candidate clock transcripts in the PSM, in order to design constructs that modulate clock period without abolishing cycling completely.

4. Experimental procedures

4.1. Generation of knock-in mice with lengthened alleles of Hes7 or Lfng

We modified the vector *pFloxRI.GCK* (supplied by the Transgenics Lab., Cancer Research UK, London Research Institute) so that it contained two multiple cloning sites (containing restriction sites SfiI, HincII, XbaI and MluI, ClaI, XhoI, NheI, Bsu36I, HindIII, respectively), one on each side of a floxed neomycin^r gene. In order to insert the transgene into the NcoI site of the 3rd *Hes7* intron, we cut the 2753 bp StuI–NcoI fragment (homology region 1: part of the *Hes7* promoter region, the first 3 *Hes7* exons, introns 1, 2 and the 5′ part of intron 3) and the 1490 bp NcoI–Bsu36I fragment (homology region 2: 3′ part of the 3rd intron, exon 4 and 3′ flanking region) from the *Hes7* locus and cloned them into the HincII–XbaI and XhoI–Bsu36I sites of the vector using short NcoI–XbaI and XhoI–NcoI DNA adapters. For the transgenic insertion into the XbaI site of the first *Lfng* intron we cut the 2123 bp BssHII–XbaI fragment (homology region 1: fragment of *Lfng* intron 1) and the 3149 bp XbaI–SacI fragment (homology region 2: 3′ part of intron 1 up to exon 8) from the *Lfng* locus and cloned them into the SfiI–XbaI and NheI–HindIII vector sites using short SfiI–BssHII and SacI–HindIII DNA adapters.

A 10,440 bp (10 kb) fragment from intron 63 of human *dystrophin* (*DMD*) was PCR-amplified (using TaKaRa LA Taq and primers acg cgt AGC CAT CTG CCC ATC TCG GCT TCC and Tat cga tTC GGT GGC TCG CGC CTG TAA TCC) from the BAC RP11–609C15 (Roswell Park Center Institute Human BAC library; GenBank Accession No.: AC078958). MluI and ClaI restriction sites were introduced via the primers (lower case bases) and used to clone the PCR product into pZErO-1 (Invitrogen) with a modified multiple cloning site and from there into the targeting vectors already containing the *Hes7* or *Lfng* homology regions. A 20,933 bp (20 kb) fragment of human *dystrophin* intron 62 was released from the same BAC by digestion with MluI, purified with a Micro Bio-Spin 30 chromatography column (Bio-Rad), and cloned into the MluI site of the *Hes7* and *Lfng* targeting vectors containing the respective homology regions. All four targeting vectors were validated.

Targeting vectors linearised with SfiI were electroporated into mouse *129/Sv* embryonic stem cells. Isolated, neo-resistant clones were screened by PCR (TaKaRa LA Taq, see Table 5 for primers) and Southern Blot analysis (for position of probes and restriction sites used see Fig. 1) for correct insertion of the transgene. Homologous recombinant stem cell clones were injected into *C57Bl/6J* blastocysts, and chimeras crossed to *C57Bl/6J* mice for germline transmission. Transgene-bearing offspring were crossed to *PGK-cre* mice to remove the floxed *neomycin^r* gene. For sequences of genotyping primers see Table 5.

4.2. Mouse lines

Knock-in mice were kept in the *C57Bl/6J* background which also served as a wildtype control. The *Lfng* null line was obtained from Randy Johnson (Evrard et al., 1998) and the *Hes7* null line from Ryoichiro Kageyama (Bessho et al., 2001b). *5kL* mice (Stauber et al., 2009) carry a randomly integrated transgene driving a chick *Lfng* cDNA (*cLfng^{cDNA}*) from a mouse *Lfng* cycling promoter. Endogenous Lfng activity was removed by repeated breeding with *Lfng* null mice. *cLfng^{cDNA}* is expressed in an oscillatory manner in wildtype and *Lfng$^{-/-}$* mice and essentially rescues the segmentation phenotype in the latter. *cLfng^{cDNA}* primary transcript is 2.5 kb long and includes a 1.3 kb 3′UTR derived from the *pLacZ-Basic* vector (Clontech). This 3′UTR contains the SV40 small *t* antigen intron and SV40 early polyadenylation signal. For comparison, the mouse *Lfng* primary transcript is 8.2 kb long and contains 7 introns. All animals were handled in strict accordance with good animal practice as defined by the Animals (Scientific Procedures) Act 1986 and in accordance with the Codes of Practice for the use of animals in scientific procedures issued by the UK Home Office.

4.3. In situ hybridization of mouse embryos

In situ hybridization of mouse embryos was performed as described (Henrique et al., 1995; Stauber et al., 2009). Probes for *Hes7* first intron, *Tbx18* and *Uncx4.1* were prepared as described in (Stauber et al., 2009); *Lfng* first intron probe as described in (Morales et al., 2002).

For the 10 kb *dystrophin* intron probe, a 913 bp fragment was PCR-amplified using the primer pair GTC CTT GTG CAA GGG TTT CTG C;CTC CCG ACC TCA AGT GAT CTG C. Riboprobes produced for the 20 kb *dystrophin* intron did not result in a staining, probably due to insufficient binding of the probe to the pre-mRNA.

4.4. Skeleton preparation

Skeletons were prepared and stained with alcian blue/alizarin red S following standard procedures. All photos were taken with a Leica DC500 digital camera and Leica Firecam version 1.7.1 software.

4.5. RT-PCR analysis of Hes7 and Lfng transcripts

Total RNA was isolated from individual E9.5 embryos of the genotypes +/+, *H10/+*, *H10/H10*, *H20/+*, *H20/H20* and *L10/L10* using the RNA Easy Kit (Qiagen). RT-PCR was carried out using the "SuperScript III One-Step RT-PCR System with Platinum Taq High Fidelity" (Invitrogen) and the following primer pairs: *Hes7*_exon1 GAGCAATGGTCACCCGGGAGCG/ *Hes7*_exon4 TCTGTAAGGCGGTGGCGGTGGC; *Hes7*_exon1 GAGCAATGGTC ACCCGGGAGCG/ 10kbDys_insert TTTTCCCATTGCCAATCAA ATGC; or *Lfng*_exon1 AGCTCCGGCTTCAGGGTCC AGG/ *Lfng*_exon4 CCGTTCTGTGGCCTGGATGGGC (following the manufacturer's instructions; 2 μl template RNA per reaction, cDNA synthesis for 30 min at 55 °C, 55 °C annealing temperature, 1 min extension time). Specific PCR products were subcloned into *pCR4-TOPO* (Invitrogen) and sequenced. Occasionally, RT-PCRs gave unspecific side products that are visible on Figs. 2K and 3E. *Hes7* exon1–exon 4 amplified a

900 bp genomic sequence from chromosome 6 containing *homeodomain-interacting protein kinase 2* (Accession No.: NT_039341). *Lfng* exon 1–exon 4 amplified a 660 bp genomic fragment from chromosome 5 containing *autism susceptibility gene 2 protein* (Accession No.: NT_039314) and a 270 bp genomic fragment from chromosome 9 containing *ribonucleoprotein PTB-binding 1* (Accession No.: NT_039472).

4.6. *High resolution episcopic microscopy*

E13.5 embryos were fixed in 4% formaldehyde in PBS and dehydrated through 30%, 50%, 60%, 90% and 100% methanol with addition of 0.275 g/100 ml eosin B in the last three steps. Samples were impregnated in 50% methanol and 50% JB4 (Polyscience) for at least 2 h, and then embedded in JB4 containing 1.25% catalyst, 0.275% eosin B and 0.055% acridine orange as per the manufacturer's instructions. Embryos were processed as described in Weninger et al. (2006) and Weninger and Mohun (2007) and <http://www.embryoimaging.org>. About 6 μm sections were imaged with a GFP filter set, and the resulting image series further processed and analysed using ImageJ. OsiriX <http://www.osirix-viewer.com> was used for the 3D reconstruction.

Acknowledgements

We thank Rippei Hayashi, Ned Hoyle and Christina Morgenstern for helpful comments on the manuscript; Ian Rosewell, the Transgenics Lab and the Biological Resources Unit (Cancer Research UK, London Research Institute) for generating and maintaining the transgenic mouse lines; Randy Johnson and Ryoichiro Kageyama for the gift of *Lfng* and *Hes7* null mice, Tim Mohun and Michael Bennett (NIMR, London) for their help with HREM, and Ahmed Mansouri for the gift of template plasmids. This research was funded by Cancer Research UK, and an Otto Hahn Medal fellowship of the Max Planck Society (to M.S.).

Appendix A. Supplementary data

Supplementary data associated with this article can be found, in the online version, at doi:10.1016/j.mod.2012.01.006.

REFERENCES

Aulehla, A., Johnson, R.L., 1999. Dynamic expression of lunatic fringe suggests a link between notch signaling and an autonomous cellular oscillator driving somite segmentation. Dev. Biol. 207, 49–61.

Aulehla, A., Wehrle, C., Brand-Saberi, B., Kemler, R., Gossler, A., Kanzler, B., Herrmann, B.G., 2003. Wnt3a plays a major role in the segmentation clock controlling somitogenesis. Dev. Cell 4, 395–406.

Aulehla, A., Wiegraebe, W., Baubet, V., Wahl, M.B., Deng, C., Taketo, M., Lewandoski, M., Pourquié, O., 2008. A beta-catenin gradient links the clock and wavefront systems in mouse embryo segmentation. Nat. Cell Biol. 10, 186–193.

Bessho, Y., Hirata, H., Masamizu, Y., Kageyama, R., 2003. Periodic repression by the bHLH factor Hes7 is an essential mechanism for the somite segmentation clock. Genes Dev. 17, 1451–1456.

Bessho, Y., Miyoshi, G., Sakata, R., Kageyama, R., 2001a. Hes7: a bHLH-type repressor gene regulated by Notch and expressed in the presomitic mesoderm. Genes Cells 6, 175–185.

Bessho, Y., Sakata, R., Komatsu, S., Shiota, K., Yamada, S., Kageyama, R., 2001b. Dynamic expression and essential functions of Hes7 in somite segmentation. Genes Dev. 15, 2642–2647.

Chipman, A.D., Akam, M., 2008. The segmentation cascade in the centipede *Strigamia maritima*: involvement of the Notch pathway and pair-rule gene homologues. Dev. Biol. 319, 160–169.

Cole, S.E., Levorse, J.M., Tilghman, S.M., Vogt, T.F., 2002. Clock regulatory elements control cyclic expression of lunatic fringe during somitogenesis. Dev. Cell 3, 75–84.

Dale, J.K., Maroto, M., Dequéant, M.L., Malapert, P., McGrew, M., Pourquié, O., 2003. Periodic notch inhibition by lunatic fringe underlies the chick segmentation clock. Nature 421, 275–278.

Darzacq, X., Shav-Tal, Y., de Turris, V., Brody, Y., Shenoy, S.M., Phair, R.D., Singer, R.H., 2007. In vivo dynamics of RNA polymerase II transcription. Nat. Struct. Mol. Biol. 14, 796–806.

Dequéant, M.L., Glynn, E., Gaudenz, K., Wahl, M., Chen, J., Mushegian, A., Pourquié, O., 2006. A complex oscillating network of signaling genes underlies the mouse segmentation clock. Science 314, 1595–1598.

Dequéant, M.L., Pourquié, O., 2008. Segmental patterning of the vertebrate embryonic axis. Nat. Rev. Genet. 9, 370–382.

Dunty Jr., W.C., Biris, K.K., Chalamalasetty, R.B., Taketo, M.M., Lewandoski, M., Yamaguchi, T.P., 2008. Wnt3a/beta-catenin signaling controls posterior body development by coordinating mesoderm formation and segmentation. Development 135, 85–94.

Evrard, Y.A., Lun, Y., Aulehla, A., Gan, L., Johnson, R.L., 1998. Lunatic fringe is an essential mediator of somite segmentation and patterning. Nature 394, 377–381.

Femino, A.M., Fay, F.S., Fogarty, K., Singer, R.H., 1998. Visualization of single RNA transcripts in situ. Science 280, 585–590.

Forsberg, H., Crozet, F., Brown, N.A., 1998. Waves of mouse lunatic fringe expression, in four-hour cycles at two-hour intervals, precede somite boundary formation. Curr. Biol. 8, 1027–1030.

Giudicelli, F., Lewis, J., 2004. The vertebrate segmentation clock. Curr. Opin. Genet. Dev. 14, 407–414.

Giudicelli, F., Ozbudak, E.M., Wright, G.J., Lewis, J., 2007. Setting the tempo in development: an investigation of the zebrafish somite clock mechanism. PLoS Biol. 5, e150.

Gomez, C., Ozbudak, E.M., Wunderlich, J., Baumann, D., Lewis, J., Pourquié, O., 2008. Control of segment number in vertebrate embryos. Nature 454, 335–339.

Gossler, A., Tam, P.P.L., 2002. Somitogenesis: segmentation of the paraxial mesoderm and the delineation of tissue compartments. In: Rossant, J., Tam, P.P.L. (Eds.), Mouse Development. Academic Press, San Diego, pp. 127–149.

Henrique, D., Adam, J., Myat, A., Chitnis, A., Lewis, J., Ish-Horowicz, D., 1995. Expression of a Delta homologue in prospective neurons in the chick. Nature 375, 787–790.

Henry, C.A., Urban, M.K., Dill, K.K., Merlie, J.P., Page, M.F., Kimmel, C.B., Amacher, S.L., 2002. Two linked hairy/enhancer of split-related zebrafish genes, her1 and her7, function together to refine alternating somite boundaries. Development 129, 3693–3704.

Hirata, H., Bessho, Y., Kokubu, H., Masamizu, Y., Yamada, S., Lewis, J., Kageyama, R., 2004. Instability of Hes7 protein is crucial for the somite segmentation clock. Nat. Genet. 36, 750–754.

Holley, S.A., Geisler, R., Nusslein-Volhard, C., 2000. Control of her1 expression during zebrafish somitogenesis by a delta-dependent oscillator and an independent wave-front activity. Genes Dev. 14, 1678–1690.

Holley, S.A., Julich, D., Rauch, G.J., Geisler, R., Nusslein-Volhard, C., 2002. Her1 and the notch pathway function within the oscillator mechanism that regulates zebrafish somitogenesis. Development 129, 1175–1183.

Jiang, Y.J., Aerne, B.L., Smithers, L., Haddon, C., Ish-Horowicz, D., Lewis, J., 2000. Notch signalling and the synchronization of the somite segmentation clock. Nature 408, 475–479.

Jouve, C., Palmeirim, I., Henrique, D., Beckers, J., Gossler, A., Ish-Horowicz, D., Pourquié, O., 2000. Notch signalling is required for cyclic expression of the hairy-like gene HES1 in the presomitic mesoderm. Development 127, 1421–1429.

Kim, W., Matsui, T., Yamao, M., Ishibashi, M., Tamada, K., Takumi, T., Kohno, K., Oba, S., Ishii, S., Sakumura, Y., Bessho, Y., 2011. The period of the somite segmentation clock is sensitive to Notch activity. Mol. Biol. Cell 22, 3541–3549.

Kraus, F., Haenig, B., Kispert, A., 2001. Cloning and expression analysis of the mouse T-box gene Tbx18. Mech. Dev. 100, 83–86.

Krol, A.J., Roellig, D., Dequeant, M.L., Tassy, O., Glynn, E., Hattem, G., Mushegian, A., Oates, A.C., Pourquié, O., 2011. Evolutionary plasticity of segmentation clock networks. Development 138, 2783–2792.

Lewis, J., 2003. Autoinhibition with transcriptional delay: a simple mechanism for the zebrafish somitogenesis oscillator. Curr. Biol. 13, 1398–1408.

Lewis, J., Hanisch, A., Holder, M., 2009. Notch signaling, the segmentation clock, and the patterning of vertebrate somites. J. Biol. 8, 44.

Mansouri, A., Yokota, Y., Wehr, R., Copeland, N.G., Jenkins, N.A., Gruss, P., 1997. Paired-related murine homeobox gene expressed in the developing sclerotome, kidney, and nervous system. Dev. Dyn. 210, 53–65.

Masamizu, Y., Ohtsuka, T., Takashima, Y., Nagahara, H., Takenaka, Y., Yoshikawa, K., Okamura, H., Kageyama, R., 2006. Real-time imaging of the somite segmentation clock: revelation of unstable oscillators in the individual presomitic mesoderm cells. Proc. Natl. Acad. Sci. USA 103, 1313–1318.

McGrew, M.J., Dale, J.K., Fraboulet, S., Pourquié, O., 1998. The lunatic fringe gene is a target of the molecular clock linked to somite segmentation in avian embryos. Curr. Biol. 8, 979–982.

Morales, A.V., Yasuda, Y., Ish-Horowicz, D., 2002. Periodic lunatic fringe expression is controlled during segmentation by a cyclic transcriptional enhancer responsive to notch signaling. Dev. Cell 3, 63–74.

Morimoto, M., Takahashi, Y., Endo, M., Saga, Y., 2005. The Mesp2 transcription factor establishes segmental borders by suppressing Notch activity. Nature 435, 354–359.

Niwa, Y., Masamizu, Y., Liu, T., Nakayama, R., Deng, C.X., Kageyama, R., 2007. The initiation and propagation of Hes7 oscillation are cooperatively regulated by Fgf and notch signaling in the somite segmentation clock. Dev. Cell 13, 298–304.

Niwa, Y., Shimojo, H., Isomura, A., Gonzalez, A., Miyachi, H., Kageyama, R., 2011. Different types of oscillations in Notch and Fgf signaling regulate the spatiotemporal periodicity of somitogenesis. Genes Dev. 25, 1115–1120.

O'Brien, T., Lis, J.T., 1993. Rapid changes in Drosophila transcription after an instantaneous heat shock. Mol. Cell Biol. 13, 3456–3463.

Oates, A.C., Ho, R.K., 2002. Hairy/E(spl)-related (Her) genes are central components of the segmentation oscillator and display redundancy with the Delta/Notch signaling pathway in the formation of anterior segmental boundaries in the zebrafish. Development 129, 2929–2946.

Palmeirim, I., Dubrulle, J., Henrique, D., Ish-Horowicz, D., Pourquié, O., 1998. Uncoupling segmentation and somitogenesis in the chick presomitic mesoderm. Dev. Genet. 23, 77–85.

Pourquié, O., 2011. Vertebrate segmentation: from cyclic gene networks to scoliosis. Cell 145, 650–663.

Pueyo, J.I., Lanfear, R., Couso, J.P., 2008. Ancestral Notch-mediated segmentation revealed in the cockroach Periplaneta americana. Proc. Natl. Acad. Sci. USA 105, 16614–16619.

Schoppmeier, M., Damen, W.G., 2005. Suppressor of Hairless and Presenilin phenotypes imply involvement of canonical Notch-signalling in segmentation of the spider *Cupiennius salei*. Dev. Biol. 280, 211–224.

Schröter, C., Oates, A.C., 2010. Segment number and axial identity in a segmentation clock period mutant. Curr. Biol. 20, 1254–1258.

Serth, K., Schuster-Gossler, K., Cordes, R., Gossler, A., 2003. Transcriptional oscillation of lunatic fringe is essential for somitogenesis. Genes Dev. 17, 912–925.

Sewell, W., Kusumi, K., 2007. Genetic analysis of molecular oscillators in mammalian somitogenesis: clues for studies of human vertebral disorders. Birth Defects Res. C Embryo Today 81, 111–120.

Shankaran, S.S., Sieger, D., Schroter, C., Czepe, C., Pauly, M.C., Laplante, M.A., Becker, T.S., Oates, A.C., Gajewski, M., 2007. Completing the set of h/E(spl) cyclic genes in zebrafish: her12 and her15 reveal novel modes of expression and contribute to the segmentation clock. Dev. Biol. 304, 615–632.

Shifley, E.T., Vanhorn, K.M., Perez-Balaguer, A., Franklin, J.D., Weinstein, M., Cole, S.E., 2008. Oscillatory lunatic fringe activity is crucial for segmentation of the anterior but not posterior skeleton. Development 135, 899–908.

Sieger, D., Tautz, D., Gajewski, M., 2004. Her11 is involved in the somitogenesis clock in zebrafish. Dev. Genes Evol. 214, 393–406.

Singh, J., Padgett, R.A., 2009. Rates of in situ transcription and splicing in large human genes. Nat. Struct. Mol. Biol. 16, 1128–1133.

Stauber, M., Sachidanandan, C., Morgenstern, C., Ish-Horowicz, D., 2009. Differential axial requirements for lunatic fringe and Hes7 transcription during mouse somitogenesis. PLoS One 4, e7996.

Stollewerk, A., Schoppmeier, M., Damen, W.G., 2003. Involvement of Notch and Delta genes in spider segmentation. Nature 423, 863–865.

Swinburne, I.A., Silver, P.A., 2008. Intron delays and transcriptional timing during development. Dev. Cell 14, 324–330.

Takashima, Y., Ohtsuka, T., Gonzalez, A., Miyachi, H., Kageyama, R., 2011. Intronic delay is essential for oscillatory expression in the segmentation clock. Proc. Natl. Acad. Sci. USA 108, 3300–3305.

Tam, P.P., Trainor, P.A., 1994. Specification and segmentation of the paraxial mesoderm. Anat. Embryol. (Berl.) 189, 275–305.

Tennyson, C.N., Klamut, H.J., Worton, R.G., 1995. The human dystrophin gene requires 16 hours to be transcribed and is cotranscriptionally spliced. Nat. Genet. 9, 184–190.

Weninger, W.J., Geyer, S.H., Mohun, T.J., Rasskin-Gutman, D., Matsui, T., Ribeiro, I., Costa Lda, F., Izpisua-Belmonte, J.C., Muller, G.B., 2006. High-resolution episcopic microscopy: a rapid technique for high detailed 3D analysis of gene activity in the context of tissue architecture and morphology. Anat. Embryol. (Berl.) 211, 213–221.

Weninger, W.J., Mohun, T.J., 2007. Three-dimensional analysis of molecular signals with episcopic imaging techniques. Methods Mol. Biol. 411, 35–46.

Zhang, N., Gridley, T., 1998. Defects in somite formation in lunatic fringe-deficient mice. Nature 394, 374–377.